

Coincidence studies of He ionized by C^{6+} , Au^{24+} , and Au^{53+} M. McGovern,¹ D. Assafrão,² J. R. Mohallem,² Colm T. Whelan,³ and H. R. J. Walters¹¹*Department of Applied Mathematics and Theoretical Physics, Queen's University, Belfast BT7 1NN, United Kingdom*²*Laboratório de Átomos e Moléculas Especiais, Departamento de Física, ICEx, Universidade Federal de Minas Gerais, Caixa postal 702, 30123-970 Belo Horizonte, MG, Brazil*³*Department of Physics, Old Dominion University, Norfolk, Virginia 23529-0116, USA*

(Received 20 January 2010; published 5 April 2010)

A recently developed [Phys. Rev. A **79**, 042707 (2009)] impact parameter coupled pseudostate approximation (CP) is applied to calculate triple differential cross sections for single ionization of He by C^{6+} , Au^{24+} , and Au^{53+} projectiles at impact energies of 100 and 2 MeV/amu for C^{6+} and 3.6 MeV/amu for Au^{24+} and Au^{53+} . For C^{6+} , satisfactory, but not perfect, agreement is found with experimental measurements in coplanar geometry, but there is substantial disagreement with data taken in a perpendicular plane geometry. The CP calculations firmly contradict a projectile-nucleus interaction model which has been used to support the perpendicular plane measurements. For Au^{24+} and Au^{53+} , there is a complete lack of accord with the available experiments. However, for Au^{24+} the theoretical position appears to be quite firm with clear indications of convergence in the CP approximation and very good agreement between CP and the completely different three-distorted-waves eikonal-initial-state (3DW-EIS) approximation. The situation for Au^{53+} is different. At the momentum transfers at which the measurements were made, there are doubts about the convergence of the CP approximation and a factor of 2 difference between the CP and 3DW-EIS predictions. The discord between theory and experiment is even greater with the experiment giving cross sections a factor of 10 larger than the theory. A study of the convergence of the CP approximation shows that it improves rapidly with reducing momentum transfer. As a consequence, lower-order cross sections than the triple are quite well converged and present an opportunity for a more reliable test of the experiment.

DOI: [10.1103/PhysRevA.81.042704](https://doi.org/10.1103/PhysRevA.81.042704)

PACS number(s): 34.50.Fa, 52.20.Hv

I. INTRODUCTION

There have been quite a number of articles, both experimental and theoretical, published on differential single ionization of He by C^{6+} projectiles [1–34]. A lesser number of papers [14,18,20,23,24,28,29,31,33,35–41] have been devoted to the more extreme system $Au^{53+} + He$ where the projectile interaction with the He target is very much stronger. Bridging the strength gap, there has also been work on single ionization of He by Au^{24+} [23,28,31,39,41]. The experimental studies have ranged from single differential cross sections to double differential cross sections, but only in recent years have fully differential measurements become available [19–24,26–28,39]. These measurements present a substantial challenge to theory as, in principle, they can show up significant discrepancies which can be hidden in less differential cross sections. However, it is a two-way street. Differences between theory and the experiment may result from flaws in the experiment or failures in the theory, or both. In the case of $C^{6+} + He$ there is a major discrepancy between the experiment and theory on measurements in a perpendicular plane at an impact energy of 100 MeV/amu [17,22]. In [17] this difference was “explained” in terms of experimental resolutions, while in [29] it is claimed that, after experimental resolutions have been taken into account, there still remains a substantial discrepancy between theory and experiment. In [42] it is suggested that this discrepancy can be attributed to elastic scattering of the projectile by the (suitably screened) He nucleus. In the case of both Au^{24+} and Au^{53+} there are substantial differences between theory and experiment [20,23,31,33,37,39]. Again, it has been suggested

that the problem lies with the experiment. On this occasion, it is sensitivity to the temperature of the He target that has been blamed [38]. Yet, under the extreme conditions presented by the Au projectiles, one must also question whether the theories that have been employed are up to the job.

The theoretical work that was carried out on the C^{6+} and $Au^{24+/53+}$ systems has been dominated by the continuum distorted-wave eikonal-initial-state approximation (CDW-EIS) [1–11,18,21,23,25,27,30–33,35,39,40], its earlier CDW incarnation [11,14,16,17,22,37], or related approximations [19,21,26,27,39,41], and by the classical trajectory Monte Carlo method (CTMC) [7,10,12–16,19,35–38]. Clearly, therefore, there is scope for a fresh approach. Recently [43–45], we developed a very powerful technique based upon an impact parameter coupled pseudostate method. In the present context this has three important advantages. First, the interaction between the projectile and the target nucleus is properly taken into account. Second, by expanding the pseudostate basis we can monitor convergence, and third, the approach is so completely different from the other methods that have previously been employed that agreement with the earlier work will be very strong support for the theoretical position.

The structure of this article is as follows. In Sec. II we give a brief outline of the theory developed in [43–45] and generalize it to the case of projectiles carrying electrons. In Sec. III computational details and conventions are described. In Sec. IV the theory is applied to $C^{6+} + He$ collisions, and in Sec. V to $Au^{24+} + He$ and $Au^{53+} + He$ collisions. In Secs. IV and V we also make a comparison with the three-distorted-waves eikonal-initial-state (3DW-EIS) approximation of [27,39], which is the most sophisticated quantal treatment to

date,¹ and as a benchmark, with the first Born approximation. Conclusions are presented in Sec. VI.

Throughout we use atomic units (a.u.) in which $\hbar = m_e = e = 1$. Unit vectors are denoted by a “hat” and complex conjugation by $*$.

II. THEORY

The theory employed here has been laid out in detail in [43–45]. According to the formulation, the amplitude for single ionization of He in a frozen-core approximation [47] is given by

$$f_{\text{ion}} = -\sqrt{\frac{2}{\pi}} v_0 \sum_{nl} (-1)^l e^{i\eta_l(\kappa)} b_{nl}(\kappa) \times \sum_{m=-l}^{m=+l} i^{m-m_0+1} C_{nlm}(q_t) e^{i(m_0-m)\phi_q} Y_{lm}(\hat{\mathbf{k}}). \quad (1)$$

In (1) it is assumed that the projectile is incident on the target He atom with relative velocity \mathbf{v}_0 and is scattered with relative velocity \mathbf{v}_f , while the ionized electron is emitted with momentum κ relative to the target nucleus. The sum is over all target states ψ_{nlm} in the set. These states can be either (approximate) eigenstates or pseudostates. Together they diagonalize the atomic Hamiltonian H_A according to

$$\langle \psi_{nlm} | H_A | \psi_{n'l'm'} \rangle = \epsilon_{nl} \delta_{nn'} \delta_{ll'} \delta_{mm'}. \quad (2)$$

The initial state of the atom is labeled $n_0 l_0 m_0$; the function $b_{nl}(\kappa)$ gives the distribution of the atom state ψ_{nlm} over the ionization continuum (see [43]); $\eta_l(\kappa)$ is the phase shift for the ejected electron scattering off its parent ion with angular momentum l ; Y_{lm} is a spherical harmonic [48] referred to \mathbf{v}_0 as the z axis; ϕ_q is the azimuthal angle of the momentum transfer $\mathbf{q} \equiv \mathbf{k}_0 - \mathbf{k}_f$ about the z axis, where $\mathbf{k}_0 = \mu \mathbf{v}_0$, $\mathbf{k}_f = \mu \mathbf{v}_f$, and μ is the reduced mass of the system. The function $C_{nlm}(q_t)$ is defined by

$$C_{nlm}(q_t) \equiv \int_0^\infty J_{(m-m_0)}(q_t b) \bar{a}_{nlm}(\infty, b) b db, \quad (3)$$

where \mathbf{q}_t is the transverse momentum transfer,

$$q_t^2 = q^2 - \frac{\mu^2(\kappa^2 + 2I)^2}{2(k_0^2 + k_f^2)}, \quad (4)$$

I is the ionization potential of the target and $J_{(m-m_0)}$ is a Bessel function.

The amplitude $\bar{a}_{nlm}(\infty, b)$ in (3) is obtained by solving coupled impact parameter equations in which the projectile moves along a straight line at impact parameter \mathbf{b} from the target. The electronic wave function of the target is expanded as [49]

$$\Psi = \sum_{nlm} a_{nlm}(t, \mathbf{b}) e^{-i\epsilon_{nl}t} \psi_{nlm}, \quad (5)$$

¹The 3DW-EIS approximation involves the sum of two terms, see equation (6) of [26]. In [46] it is shown that for heavy particle impact at high energies, when the impact parameter approximation is valid, this second term is negligible. Consequently, under these circumstances it would appear that 3DW-EIS differs from CDW-EIS only in the use of a Hartree-Fock description of the initial and final states of the ionized target electron.

leading to the coupled equations

$$i \frac{d a_{nlm}}{dt} = \sum_{n'l'm'} e^{i(\epsilon_{nl} - \epsilon_{n'l'})t} \langle \psi_{nlm} | V | \psi_{n'l'm'} \rangle a_{n'l'm'}, \quad (6)$$

where V is the interaction between the projectile and the target. When the projectile is a bare ion with charge Z_P

$$V = Z_P \left(\frac{Z_T}{R} - \sum_{i=1}^{Z_T} \frac{1}{|\mathbf{R} - \mathbf{r}_i|} \right), \quad (7)$$

where Z_T is the charge on the target nucleus and \mathbf{R} (\mathbf{r}_i) is the position vector of the projectile (i th target electron) relative to the target nucleus. For the Au projectiles considered here we must generalize to the case where the projectile carries electrons. Let the projectile have nuclear charge Z_P and contain N_P ($< Z_P$) electrons and let its electronic state be described by a single Slater determinant composed out of orthonormal spin orbitals whose spatial components are given by $\chi_{NL}(r) Y_{LM}(\hat{\mathbf{r}})$ where \mathbf{r} is the position vector of a projectile electron relative to the projectile nucleus. We make a static screening approximation. Let $V_{\text{static}}(\mathbf{X})$ be the static potential of the projectile as seen by a unit positive charge at position \mathbf{X} relative to the projectile nucleus. Then

$$V_{\text{static}}(\mathbf{X}) = \frac{Z_{\text{res}}}{X} + \sum_{NLM} \mu_{NLM} \int \chi_{NL}(r) Y_{LM}^*(\hat{\mathbf{r}}) \times \left(\frac{1}{X} - \frac{1}{|\mathbf{X} - \mathbf{r}|} \right) \chi_{NL}(r) Y_{LM}(\hat{\mathbf{r}}) r^2 dr d\hat{\mathbf{r}}, \quad (8)$$

where

$$Z_{\text{res}} = Z_P - N_P, \quad (9)$$

is the residual charge on the projectile and μ_{NLM} ($= 0, 1, \text{ or } 2$) is the spin occupancy of the spatial orbital NLM . We spherically average this potential to get

$$V_{\text{static}}(X) = \frac{Z_{\text{res}}}{X} + \sum_{NL} \Gamma_{NL} \int_X^\infty \chi_{NL}(r) \times \left(\frac{1}{X} - \frac{1}{r} \right) \chi_{NL}(r) r^2 dr, \quad (10)$$

where Γ_{NL} is the number of electrons in the NL shell. The potential V_{static} consists of a Coulombic component and a short-range part V_{SR}

$$V_{\text{static}}(X) = \frac{Z_{\text{res}}}{X} + V_{SR}(X). \quad (11)$$

For the interaction between the projectile and target we take

$$V = Z_{\text{res}} \left(\frac{Z_T}{R} - \sum_{i=1}^{Z_T} \frac{1}{|\mathbf{R} - \mathbf{r}_i|} \right) + Z_T V_{SR}(R) - \sum_{i=1}^{Z_T} V_{SR}(|\mathbf{R} - \mathbf{r}_i|). \quad (12)$$

Once f_{ion} is determined the triple differential cross section (TDCS) in the laboratory frame may be calculated from [43]

$$\frac{d^3 \sigma^L}{dE d\Omega_e d\Omega_p} = \frac{v_f \kappa}{v_0} m_p^2 |f_{\text{ion}}|^2, \quad (13)$$

where m_P is the mass of the projectile. This is the cross section for the projectile being scattered into the solid angle $d\Omega_P$ in the laboratory while the ionized electron is ejected into the solid angle $d\Omega_e$ with energy in the range E to $E + dE$. From (13) lower-order cross sections can be calculated by integration as described in [43–45].

III. COMPUTATIONAL DETAILS AND CONVENTIONS

In the strict form of the approximation (1) described in [43] the set of states ψ_{nlm} is constructed so that there is one state $v = n$ of each angular symmetry lm corresponding to the ionized energy, that is,

$$\epsilon_{vl} = \frac{\kappa^2}{2} + I + \epsilon_0. \quad (14)$$

It is then found that $b_{nl}(\kappa)$ is negligible except for $n = v$ and so the sum over n in (1) reduces to the single case $n = v$. In this article we consider four ejected electron energies: 1, 4, 6.5, and 10 eV. We have therefore constructed a different set of states for each of these cases.

As in [43] we adopt a frozen target approximation and construct the He states ψ_{nlm} from a basis

$$\frac{1}{\sqrt{2}} [\chi_{klm}(\mathbf{r}_1)\phi_{1s}^+(r_2) + \chi_{klm}(\mathbf{r}_2)\phi_{1s}^+(r_1)] \\ k = 1 \text{ to } (2l - 1), \quad l = 0 \text{ to } 9, \quad (15)$$

where ϕ_{1s}^+ is the $1s$ orbital of He⁺ and

$$\chi_{nlm}(\mathbf{r}) = (\lambda_l r)^l L_{k-1}^{2l+2}(\lambda_l r) e^{-\lambda_l r/2} Y_{lm}(\hat{\mathbf{r}}), \quad (16)$$

where L_{k-1}^{2l+2} is a Laguerre polynomial. This gives 165 states in total. For the 1 eV set we have chosen [50] the $n = 7$ states to satisfy (14); for the 4 and 6.5 eV sets, the $n = 10$ states; and for the 10 eV set, the $n = 11$ states. For 1 eV ejection there are no $n = 7$ states for $l = 7, 8$, and 9 . In these cases the state $(n, l = n - 1)$ has been constructed to have the same energy as the state $(n, l = n - 2)$ for $n = 8, 9$, and 10 .

To assess convergence we also used 75 state sets where k runs from 1 to $(15 - l)$ and l from 0 to 5. For the 1 eV set the $n = 5$ states satisfy (14); for 4 and 6.5 eV, the $n = 7$ states; and for 10 eV, the $n = 8$ states. Again, for the 1 eV set we have taken the $n = 6, l = 5$ state to have the same energy as the $n = 6, l = 4$ state.

The strict form of the approximation (1) described previously is inconvenient where we wish to study a large range of ejected energies or cross sections such as $d\sigma/d\Omega_e$, which involve integration over all ejected energies. In [44,45] it was shown that the generalized approximation (1), where we use a single set of states ψ_{nlm} for a range of ejected energies, performs well. In the calculations reported here, which are not for a specific ejected energy, we used (1) with the 4 eV set of states.

A very useful benchmark is the first Born approximation. For C⁶⁺ + He collisions we made first Born calculations that are effectively exact within the frozen-target approximation (see [43]). We label these as exact first Born approximation (EXB1). For the Au^{24+/53+} + He collision systems because of the need to take electron shielding of the projectile nucleus into account, we used the first Born approximation as calculated

in the impact parameter pseudostate approximation (IPMB1) (see [43]). How close IPMB1 is to the exact first Born approximation depends upon the quality of the pseudostate set used. By comparing calculations of IPMB1 with different sets of pseudostates we get some measure of the relative quality of the sets. Unless otherwise stated, our IPMB1 results were evaluated with the 165 state sets. Experience with this size of expansion [43–45] indicates that highly accurate first Born cross sections can be so obtained.

At the high impact energies studied here it is important to include a large enough range of impact parameters. The adequacy of the range can be judged by monitoring the change in the cross section as the range is increased, or better still, by comparing IPMB1 numbers with the EXB1. A particularly sensitive test is to compare the TDCS in the IPMB1 approximation with that in EXB1 in the plane perpendicular to the momentum transfer \mathbf{q} . In this plane the first Born approximation to the TDCS must be constant and also takes on its smallest value. Such a test applied to C⁶⁺ impact on He at 100 MeV/amu suggested that we should take the impact parameter range in this case up to 250 a.u.. For C⁶⁺ impact at 2 MeV/amu we used impact parameters up to 80 a.u., and for Au²⁴⁺ and Au⁵³⁺ at 3.6 MeV/amu, up to 120 a.u..

In the experimental work with Au²⁴⁺ and Au⁵³⁺ [18,20,23,24,28,29,35,39] the electronic state of the projectile is not defined. We assumed that these projectiles are in their ground-state configurations. These are, respectively,

$$\text{Au}^{24+}(1s^2 2s^2 2p^6 3s^2 3p^6 3d^{10} 4s^2 4p^6 4d^{10} 4f^9), \quad (17)$$

and

$$\text{Au}^{53+}(1s^2 2s^2 2p^6 3s^2 3p^6 3d^8). \quad (18)$$

To evaluate (10) we used the nonrelativistic Roothan-Hartree-Fock results for the doublet S ground state of neutral Au given in [51].

In displaying our results we adopt the following conventions. We take the Z direction to be the direction of the incident projectile. The incident and scattered projectile define the X - Z plane with the scattered projectile coming out on the negative X side. This Cartesian coordinate system is completed with a Y axis to form a right-handed set. In this article we study electron ejection in the X - Z plane (coplanar geometry) and in the Y - Z plane (perpendicular plane geometry). In these geometries we adopt the convention that angles are measured from the Z axis with those in the positive (negative) X or Y half-plane lying in the range 0° to 180° (0° to -180°).

Finally, we label the full impact parameter coupled pseudostate calculations as CP.

IV. C⁶⁺ + He COLLISIONS

In this section we compare our calculations with the experimental data at impact energies of 100 [22] and 2 MeV/amu [27].

Before addressing individual cases, we note from Figs. 1 to 3 that there is excellent agreement between the 75 state and 165 state CP calculations in all cases. The agreement is so good that, even with the color coding in the online versions of these figures, it is difficult to tell the difference between the

two approximations. This close agreement implies very good convergence.

A. 100 MeV/amu impact energy, 6.5 eV ejected electron energy

In Fig. 1(a) we compare our CP and EXB1 TDCS's with the experimental data of [22] (see also [17]) in coplanar geometry. The impact energy is 100 MeV/amu, the momentum transfer is $q = 0.75$ a.u., and the ejection energy is 6.5 eV. There is good, although not perfect, agreement between the CP calculation and the experimental data. In the figure we see the classic binary and recoil peaks associated with the high-energy regime. It is also clear from the figure that the CP approximation is very close to the first Born result (i.e., we are very much in the first-order perturbation regime).

Figure 1(b) shows the TDCS in the Y - Z plane. Since the scattering plane is the X - Z plane, in this geometry the cross section should be symmetric about 0° . The momentum transfer q in Fig. 1(b) is again 0.75 a.u.. In this case the momentum transfer vector makes an angle of 88.6° with the Z

axis. Thus the Y - Z plane is almost the plane perpendicular to \mathbf{q} and has been referred to as such in the literature [22]. If the Y - Z plane were the plane exactly perpendicular to \mathbf{q} , then the first Born cross section, which is symmetric about \mathbf{q} , would be constant in this geometry. This is almost true of the EXB1 curve in Fig. 1(b), which shows a small minimum at 0° . The CP approximation shows more variation, but nothing comparable to that seen in the experimental data. Fiol *et al.* [17] argued that the large variation in the experimental data can be explained by taking account of experimental resolutions. However, Schulz *et al.* [42] claimed that only at most 50% of the structure in the experimental data can be accounted for by experimental resolution (i.e., at least 50% of the structure is dynamical in origin). A number of theories have been constructed which support this interpretation [34,42]. These theories explain the effect as a result of elastic scattering of the C^{6+} projectile by the He nucleus. However, the theories are not firmly based, and unlike the CP approximation, do not incorporate the nuclear scattering in a consistently derived approximation from basic quantum scattering theory. The CP approximation, which was shown in [43] to take account of nuclear scattering and which is well founded in its derivation from a proper wave treatment, firmly contradicts this explanation.

B. 2 MeV/amu impact energy

In Fig. 2 we compare our CP and EXB1 results with the measurements reported in [27] in coplanar geometry for ejected electron energies of 1, 4, and 10 eV and for momentum transfers q of 0.45, 0.65, 1.0, and 1.5 a.u.. While there are obvious differences between the CP calculations and the experiment, the overall agreement between the two is reasonable. One noteworthy difference is the infilling, in the experimental data, of the minimum near 0° between the binary and recoil peaks at the lower momentum transfers of $q = 0.45$ and 0.65 a.u.. Taken at face value, this would seem to imply that the outgoing C^{6+} tends to drag the ejected electron behind it to a greater extent than predicted by theory [i.e., a larger post collisional interaction (PCI)].

Figure 3 compares the CP cross sections with the 3DW-EIS theory of Foster *et al.* [27], again in the presence of the experimental data. We see quite good agreement between the two theories although there seems to be some drift between them with an increasing momentum transfer. That such good agreement can be obtained with such a different theory as 3DW-EIS adds strong support to the CP results.

Finally, in Fig. 4 we show three-dimensional pictures of the EXB1 and CP triple differential cross sections for electron ejection at 4 eV. We see that, at the lowest momentum transfer shown, $q = 0.45$ a.u., the CP and EXB1 cross sections are comparable in size except that, as expected, the binary peak of the CP approximation becomes larger than the EXB1 binary peak and the CP recoil peak becomes smaller than that of EXB1, the two CP peaks being bent toward the outgoing C^{6+} (i.e., PCI). At these momentum transfers we are not far away from the perturbative first Born regime. However, with increasing momentum transfer q the CP TDCS becomes smaller than that of EXB1 until at the highest momentum transfer shown, $q = 1.5$ a.u., it is substantially smaller. Here,

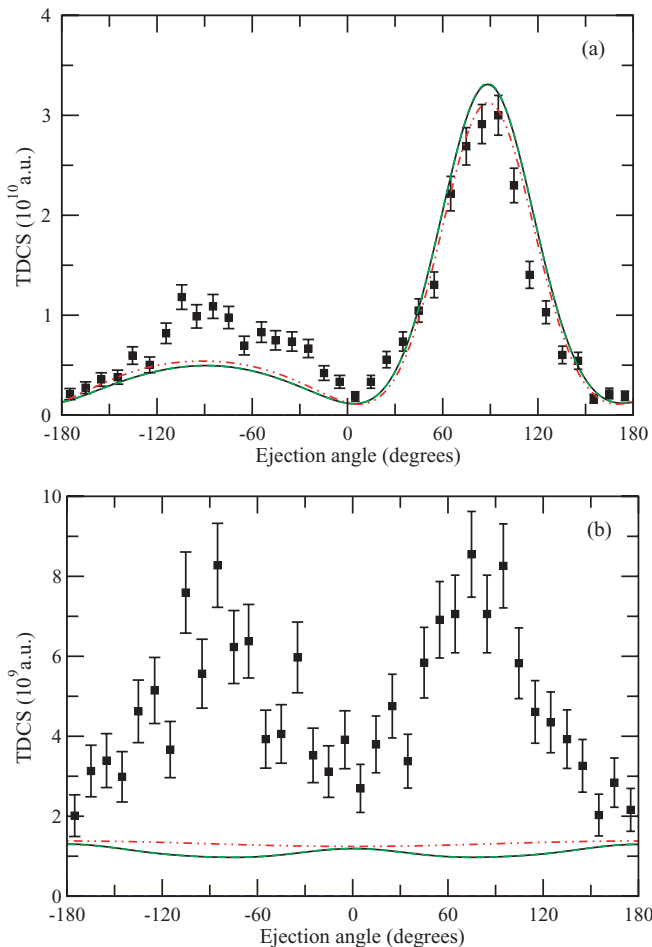


FIG. 1. (Color online) TDCS at 100 MeV/amu, $q = 0.75$ a.u., and an ejected electron energy of 6.5 eV in (a) coplanar geometry, (b) the Y - Z plane: solid black curve, 165 state CP approximation; dashed green curve*, 75 state CP approximation; dash-double-dot red curve, EXB1; experimental data from [17,22].

*Note that in a black and white version of this figure the dashed green curve is indistinguishable from the solid black curve.

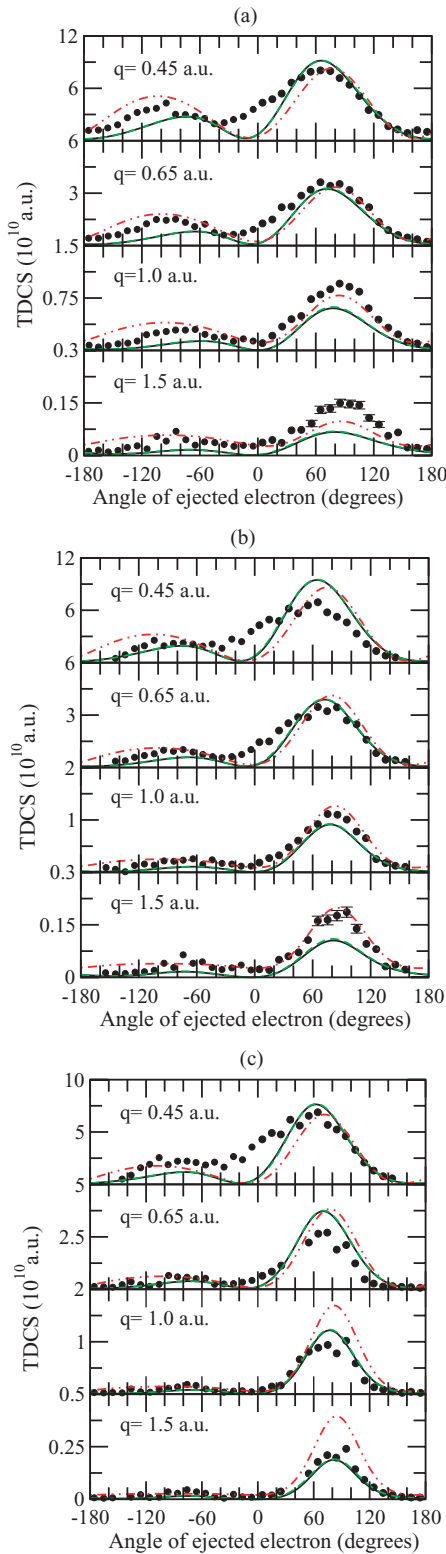


FIG. 2. (Color online) Coplanar TDCS at 2 MeV/amu and ejected electron energy of (a) 1 eV, (b) 4 eV, and (c) 10 eV: solid black curve, 165 state CP approximation; dashed green curve*, 75 state CP approximation; dash-double-dot red curve, EXB1; experimental data from [27].

*Note that in a black and white version of this figure the dashed green curve is indistinguishable from the solid black curve.

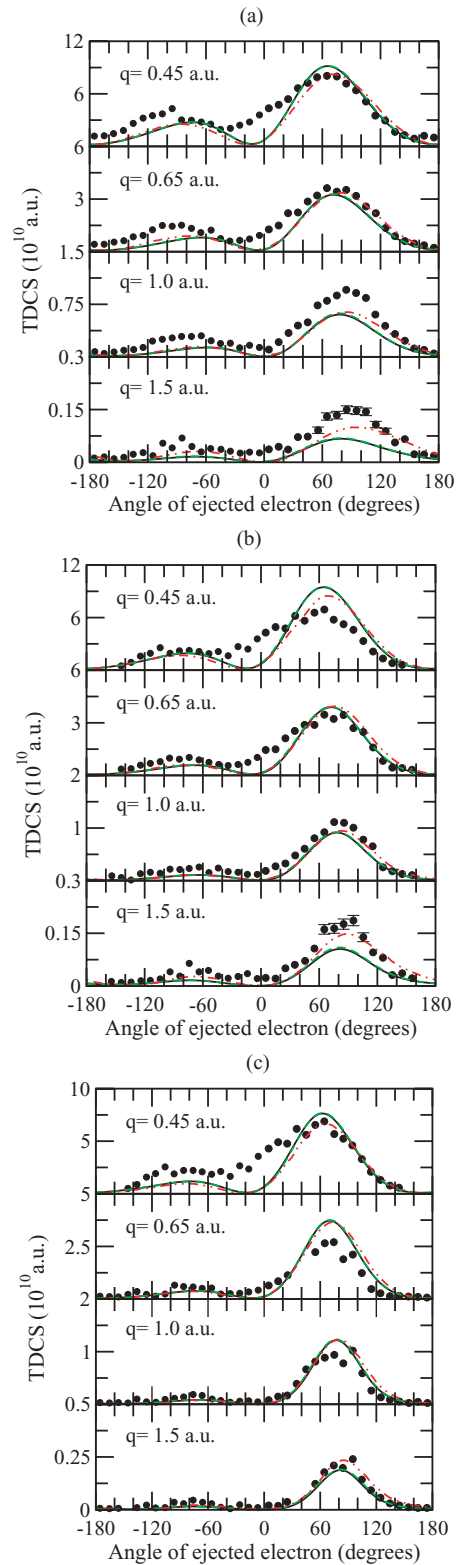


FIG. 3. (Color online) As in Fig. 2 except that the dash-double-dot red curve is now the 3DW-EIS approximation of [27].

we are now well away from the first-order perturbative region. This is not surprising in that large momentum transfers imply close collisions and so the 6+ charge on

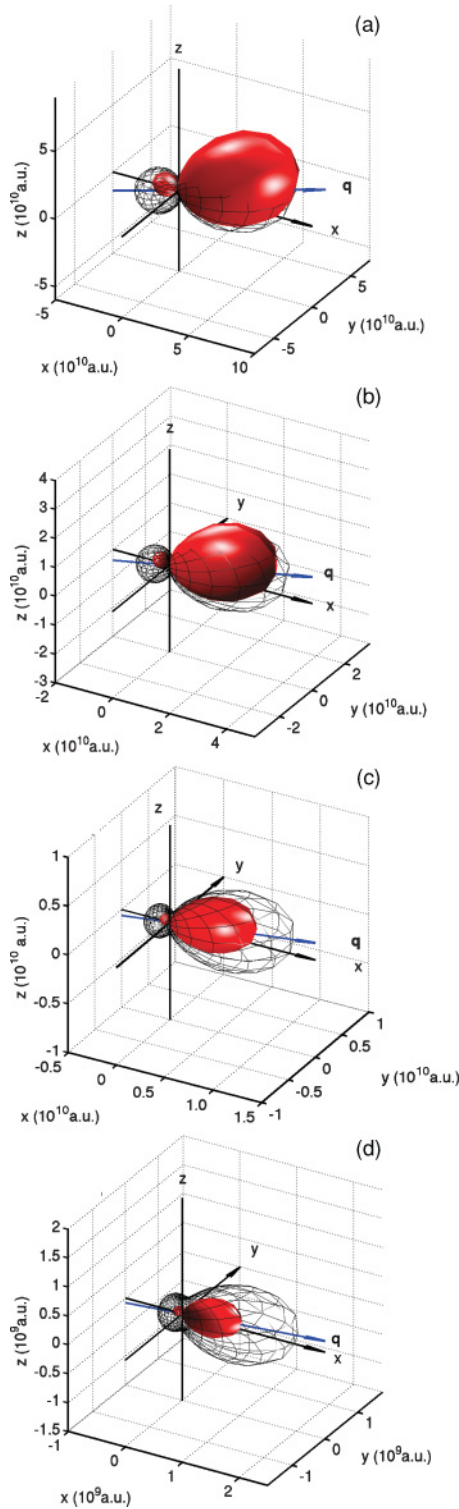


FIG. 4. (Color online) TDCS at 2 MeV/amu and for an ejected electron energy of 4 eV at (a) $q = 0.45$ a.u., (b) $q = 0.65$ a.u., (c) $q = 1.0$ a.u., and (d) $q = 1.5$ a.u.: solid surface, 165 state CP approximation; wire cage, EXB1.

the C begins to have a stronger effect on the He electrons. The three-dimensional pictures of Fig. 4 emphasize this point more strongly than the corresponding coplanar cuts of Fig. 2(b).

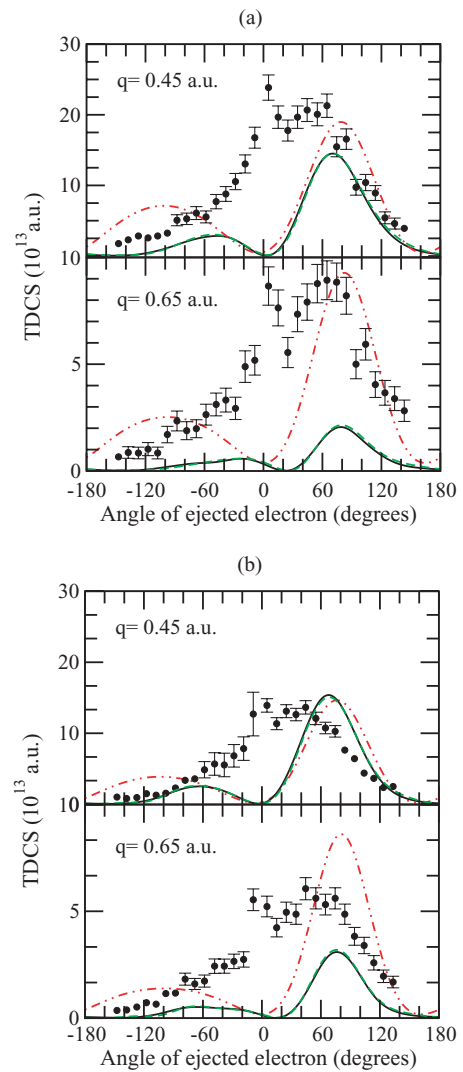


FIG. 5. (Color online) Coplanar TDCS for ejection of (a) a 4 eV electron, (b) a 10 eV electron, by Au^{24+} impact on He at 3.6 MeV/amu; solid black curve, 165 state CP approximation; dashed green curve*, 75 state CP approximation; dash-double-dot red curve, $\text{IPMB1} \times 0.5$; experimental data from [39].

*Note that in a black and white version of this figure the dashed green curve is indistinguishable from the solid black curve.

Similar behavior is seen for electron ejection at 1 and 10 eV [45].

V. $\text{AU}^{24+} + \text{HE}$ AND $\text{AU}^{53+} + \text{HE}$ COLLISIONS AT 3.6 MEV/AMU

A. Triple differential cross sections

In Fig. 5 we show the TDCS for ionization of He by Au^{24+} at an impact energy of 3.6 MeV/amu, for ejected electron energies of 4 and 10 eV and for momentum transfers of 0.45 and 0.65 a.u.. The geometry is coplanar. The first thing to observe from Fig. 5 is the excellent agreement between the 75 and 165 state CP calculations. This implies convergence of our results. Also shown is the IPMB1 first Born approximation, which has been reduced by a factor

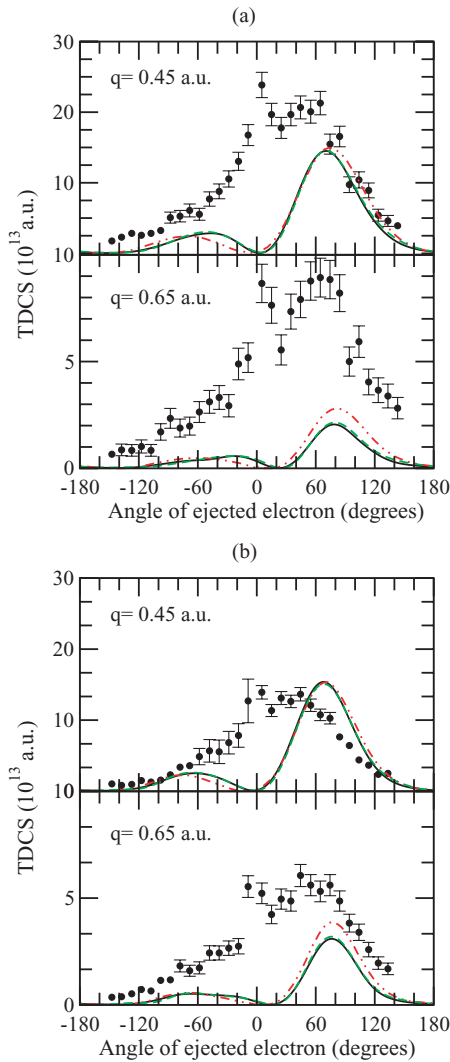


FIG. 6. (Color online) As in Fig. 5 except that the red dash-double-dot red curve is now the 3DW-EIS approximation of Foster *et al.* [39].

of 2 to fit it onto the same scale. Clearly we are now far away from the first-order perturbative limit. Both the CP and IPMB1 results show clear binary and recoil peaks. The same cannot be said of the experimental data, which seem to indicate that the ejected electron is being dragged behind the outgoing Au²⁴⁺. The agreement with the experiment is not good. Some comfort is derived from Fig. 6, which compares the 3DW-EIS approximation of Foster *et al.* [39] with our CP approximation and experiment. Here we see very reasonable agreement between the two theories. In view of the agreement between the three approximations, 75 state CP, 165 state CP, and 3DW-EIS, we are inclined to suggest that it may not be the theory that is at fault. Indeed, Olson and Fiol [38] suggested that there may be extreme sensitivity to the temperature profile of the target gas jet.

Figure 7 shows our results for ionization of He by Au⁵³⁺ at 3.6 MeV/amu, ejected electron energies of 4 and 10 eV, and momentum transfers of 0.65 and 1.0 a.u.. Again, the geometry is coplanar. Unlike the case of Au²⁴⁺ we now see significant

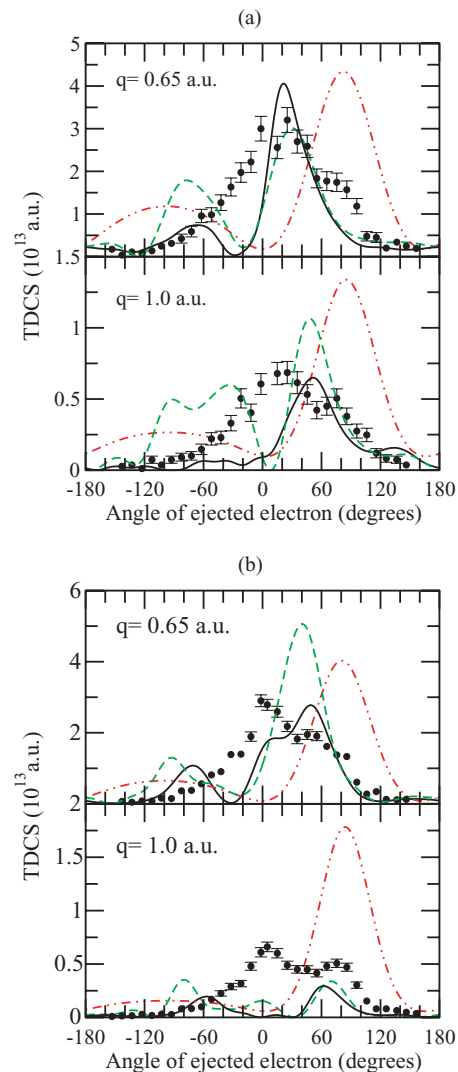


FIG. 7. (Color online) Coplanar TDCS for ejection of (a) a 4 eV electron, (b) a 10 eV electron, by Au⁵³⁺ impact on He at 3.6 MeV/amu: solid black curve, 165 state CP approximation; dashed green curve, 75 state CP approximation; dash-double-dot red curve, IPMB1 $\times 0.05$; experimental data $\times 0.1$ from [39].

differences between the 75 state and 165 state CP calculations. Clearly, the 75 state calculation has not converged, and doubt is therefore cast upon the convergence of the 165 state results. There is little agreement with the shape of the experimental data, but the major disagreement with the experiment is on normalization. To fit the experimental data onto Fig. 7 we normalized the points downward by a factor of 10. Figure 7 also shows the first Born IPMB1 approximation, which has been normalized downward by a factor of 20 to fit onto the figure. Clearly, we are now very far away from the perturbative limit. Figure 8 compares our results with the 3DW-EIS calculations of Foster *et al.* [39], there is some measure of agreement between the 165 state CP approximation and the 3DW-EIS result except that the latter, as shown in Fig. 8, has been scaled up by a factor of 2.

The difference between the Au²⁴⁺ and Au⁵³⁺ outcomes is marked. Whereas the theories are in reasonable agreement for Au²⁴⁺, and so we may have some confidence in them, the

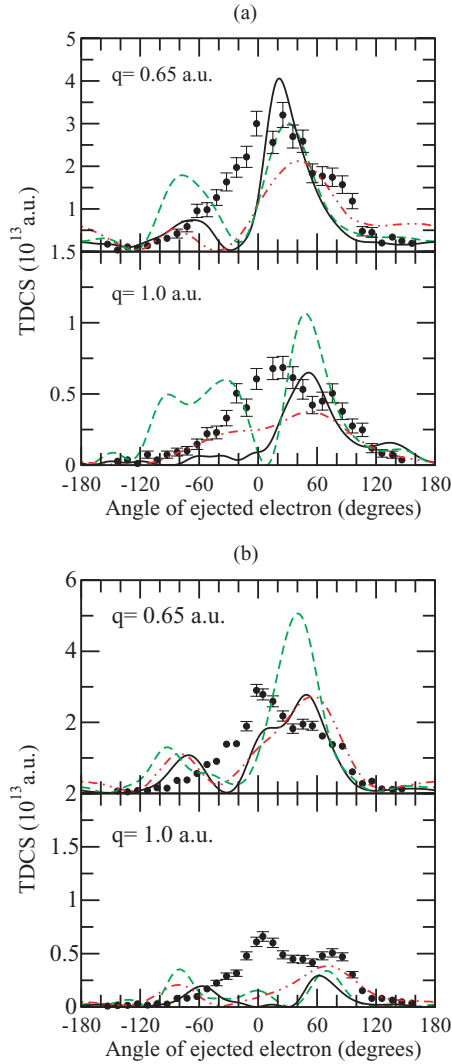


FIG. 8. (Color online) As in Fig. 7 except, dash-double-dot red curve is 3DW-EIS approximation $\times 2$ of Foster *et al.* [39].

theoretical results for Au^{53+} are at odds with each other. Let us investigate this issue further.

Figure 9 (and later Fig. 12) throws some interesting light upon the convergence of the CP approximation. Figure 9 is a continuation of Fig. 7(a) for Au^{53+} to lower momentum transfers. Here we see the 75 state and 165 state CP approximations coming into agreement with reducing momentum transfer (i.e., convergence depends upon the momentum transfer). This makes sense in that larger momentum transfers imply closer collisions and therefore a stronger interaction between the projectile and the target. This is also consistent with the observation from Fig. 9 that the CP cross section becomes comparable in magnitude to the first Born cross section (IPMB1) with reducing momentum transfer (i.e., the first-order perturbative limit is approached as the interaction between the projectile and the target weakens). It should also be noted from Figs. 7(a), 9, and 12 how quickly the magnitude of the CP cross section declines with increasing momentum transfer. The experimental measurements reported in Figs. 5 to 8 have been made at momentum transfers where the cross section is, relatively speaking, small.

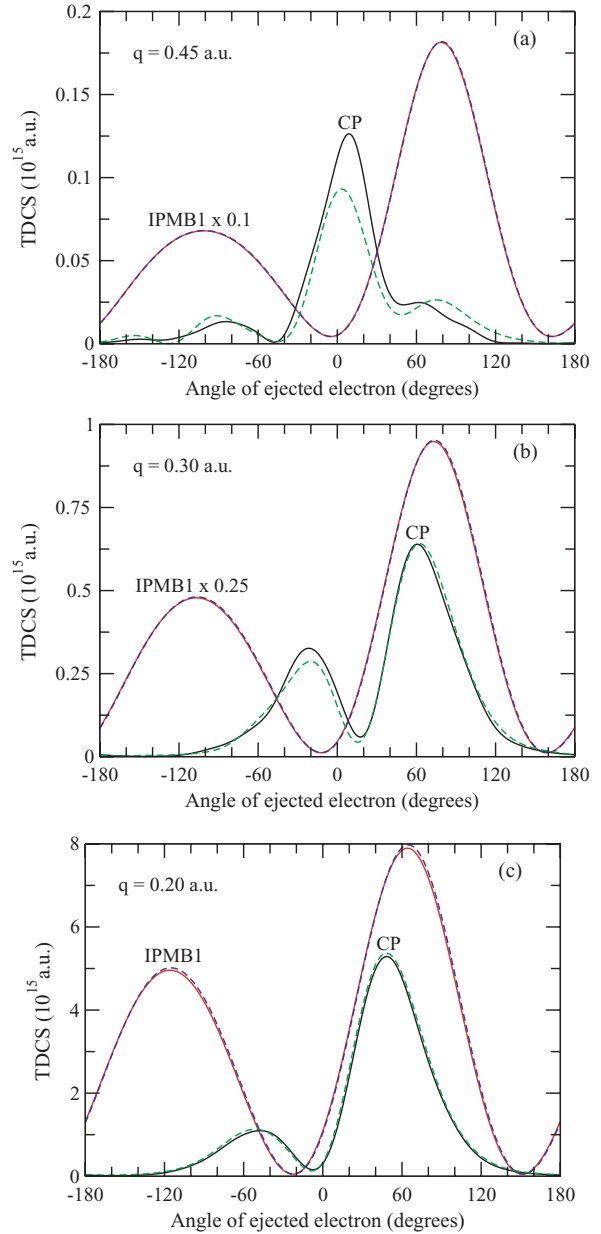


FIG. 9. (Color online) Coplanar TDCS for ejection of a 4 eV electron by Au^{53+} impact on He at 3.6 MeV/amu: solid curves (CP and IPMB1), 165 state approximation; dashed curves (CP and IPMB1), 75 state approximation.

It is interesting to see the TDCS's in full three dimensions. These are shown in Figs. 10 and 11 for an electron ejection energy of 4 eV and for momentum transfers q between 0.125 and 0.65 a.u.. The cross sections have been calculated in the 165 state CP approximation. At $q = 0.125$ a.u., where the cross section is dominated by long-range interactions, the cross sections have the classic shape, as already seen for C^{6+} in Fig. 4, of a well-defined binary and recoil peak. Like C^{6+} , these peaks are bent upward toward the outgoing attracting ion, the amount of bending increasing with the charge on the ion. This basic shape, although gradually modified with increasing q , is retained by Au^{24+} up to $q = 0.65$ a.u.. The Au^{53+} cross section at $q = 0.30$ a.u. is similar to that of Au^{24+} at $q = 0.65$ a.u.

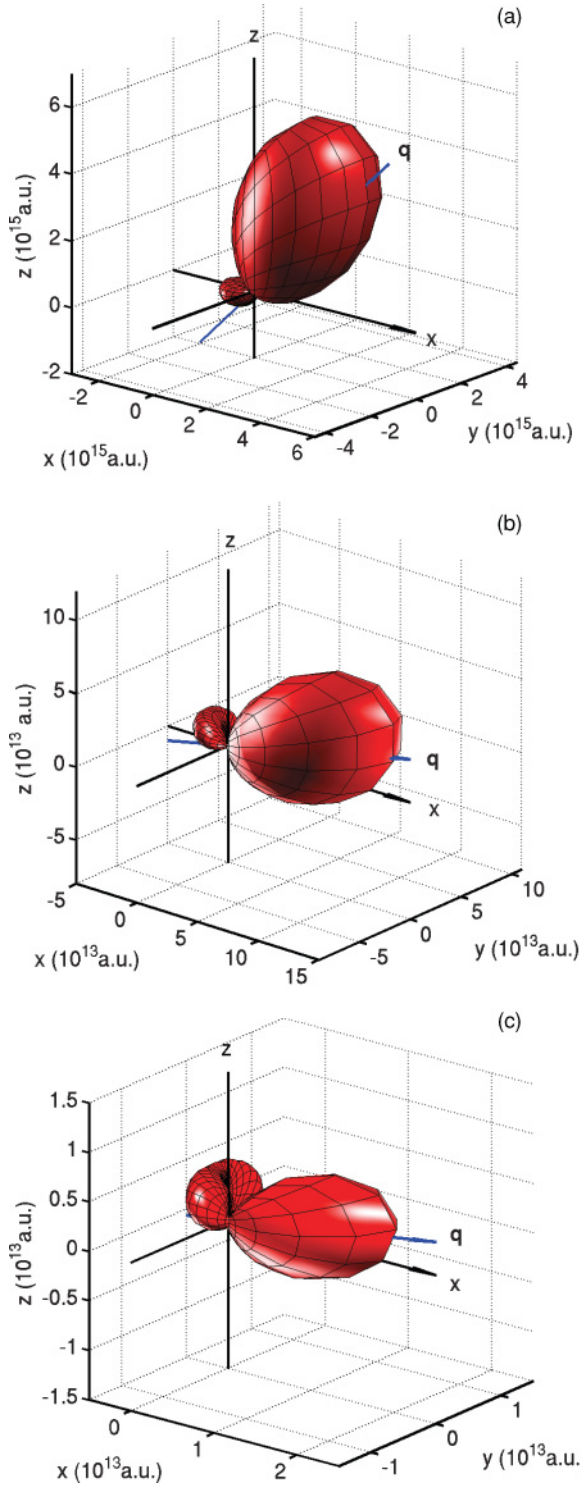


FIG. 10. (Color online) TDCS in the 165 state CP approximation for ejection of a 4 eV electron by Au²⁴⁺ impact on He at (a) $q = 0.125$ a.u., (b) $q = 0.45$ a.u., and (c) $q = 0.65$ a.u..

but is more bent. By $q = 0.45$ a.u. the Au⁵³⁺ cross section has completely changed and indicates a strong tendency for the ejected electron to follow the outgoing ion. The marked decrease in the magnitude of the TDCS with increasing q is again to be noted.

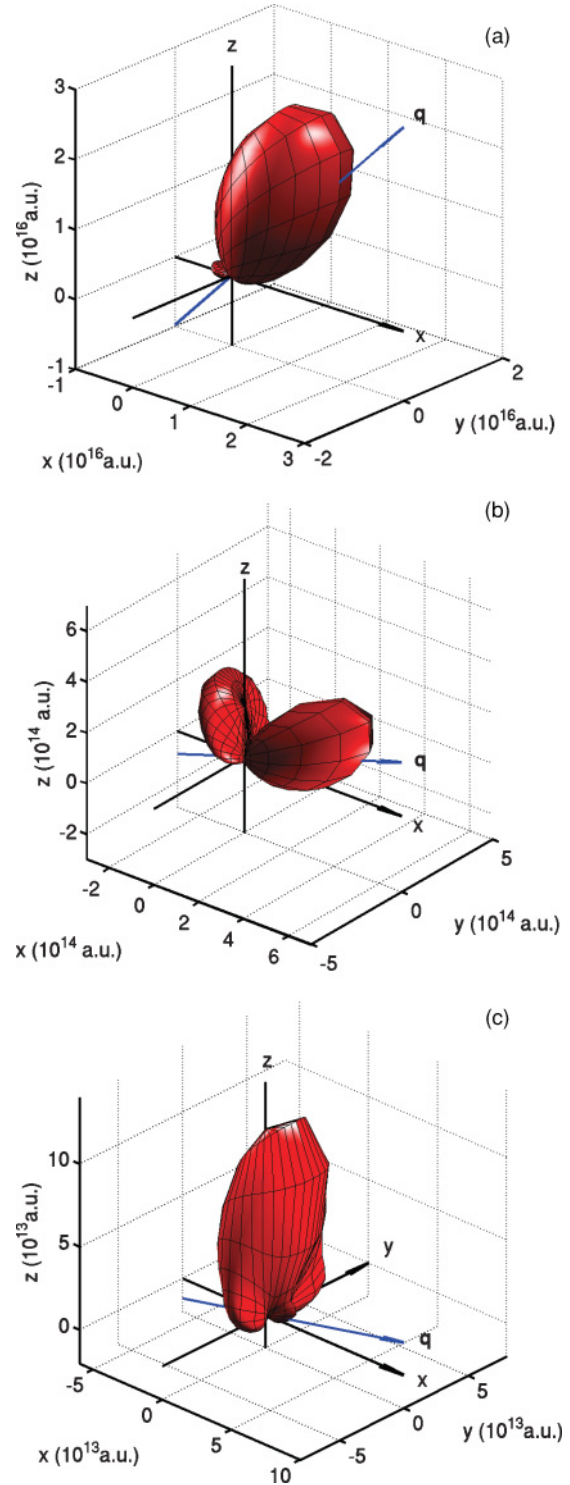


FIG. 11. (Color online) TDCS in the 165 state CP approximation for ejection of a 4 eV electron by Au⁵³⁺ impact on He at (a) $q = 0.125$ a.u., (b) $q = 0.30$ a.u., and (c) $q = 0.45$ a.u..

B. Double differential cross sections

1. $d^2\sigma/dEdq$

Figure 12 shows the double differential cross section $d^2\sigma/dEdq$ for Au²⁴⁺ and Au⁵³⁺ in the CP and IPMB1 approximations for ejected electron energies of 4 and 10 eV. In each case both 75 and 165 state calculations are shown.

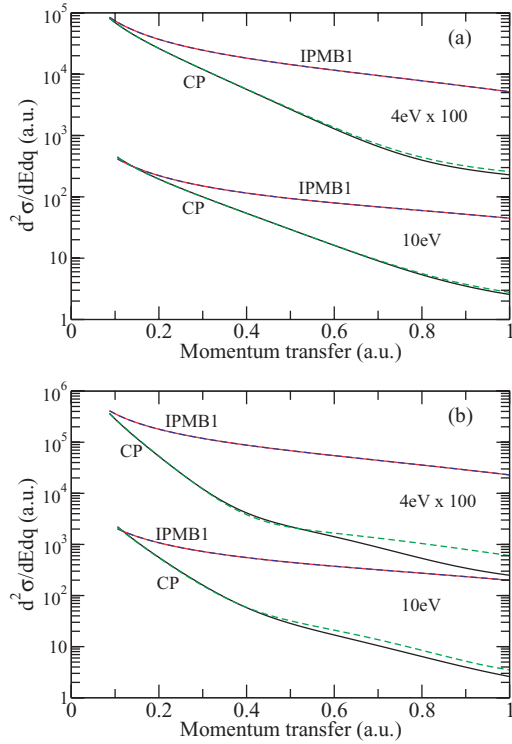


FIG. 12. (Color online) $d^2\sigma/dEdq$ for impact of (a) Au^{24+} and (b) Au^{53+} , on He at 3.6 MeV/amu for ejected electron energies of 4 and 10 eV: solid curves (CP and IPMB1), 165 state approximation; dashed curves (CP and IPMB1), 75 state approximation.

For IPMB1 these two calculations are in good agreement with each other. For CP there is divergence between them with increasing momentum transfer q . In the case of Au^{24+} the divergence is small in the momentum transfer range shown, but for Au^{53+} it is very noticeable. The divergence results from the growing strength of the average interaction between the projectile and the target with increasing q , as a result of closer collisions, and the consequent need for a better representation of the collision wave function. With decreasing q , not only do the 75 and 165 state CP cross sections converge, but also the CP and IPMB1 cross sections. In the limit of small q the effective interaction becomes weaker and the first-order perturbative limit is approached. Notice the large reduction in magnitude of the CP cross section with increasing q and observe that the experimental measurements reported in Figs. 5 to 8 have been made where the cross section is relatively small.

2. $d^2\sigma/dEd\Omega_e$

In Fig. 13 we show the 75 state and 165 state results for $d^2\sigma/dEd\Omega_e$ for the ejected electron energies of 4 and 10 eV. Here we do see a small difference between the 75 state and 165 state calculations of IPMB1. A similar difference is seen in the CP cross sections except for the case of Au^{53+} at 4 eV ejection where the excursion between the two cross sections is a little bit larger. Generally, however, Fig. 13 suggests that the 165 state results should be quite good.

The IPMB1 cross sections display a peak near 80° corresponding to the first Born TDCS binary peak averaged

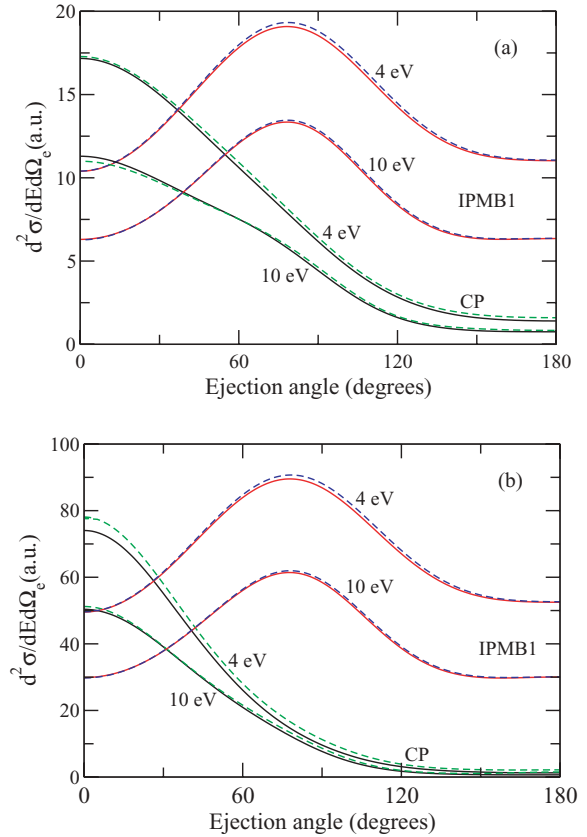


FIG. 13. (Color online) $d^2\sigma/dEd\Omega_e$ for impact of (a) Au^{24+} and (b) Au^{53+} , on He at 3.6 MeV/amu for ejected electron energies of 4 and 10 eV: solid curves (CP and IPMB1), 165 state approximation; dashed curves (CP and IPMB1), 75 state approximation.

over all scattered projectile directions. The CP cross sections are completely different, indicating a steady rise from the backward direction to the forward direction. This is a result of the postcollisional interaction between the ejected electron and the outgoing Au ion which drags the electron behind it. For 10 eV ejection under Au^{24+} impact, Fig. 13(a), there is a small change in curvature of the cross section near 70° . This seems to be a contest between the postcollisional interaction and the binary peak structure that is seen in the IPMB1 cross sections. We shall see this competition again in Fig. 15. As would be expected from the greater postcollisional interaction, the cross sections for Au^{53+} rise more steeply from the backward direction to the forward direction than for Au^{24+} .

Figure 14 shows three-dimensional plots of $d^2\sigma/dEd\Omega_e$ for Au^{24+} and Au^{53+} impact at 3.6 MeV/amu calculated in the 165 state CP approximation. This figure shows that low-energy electrons are strongly pulled out at the forward direction and even for energies as high as 40 eV the electrons are mainly ejected into the forward cone.

C. Single differential cross sections

1. $d\sigma/d\Omega_e$

Figure 15 shows the CP and IPMB1 results for $d\sigma/d\Omega_e$ in the 75 and 165 state approximations. As in Fig. 13, the first

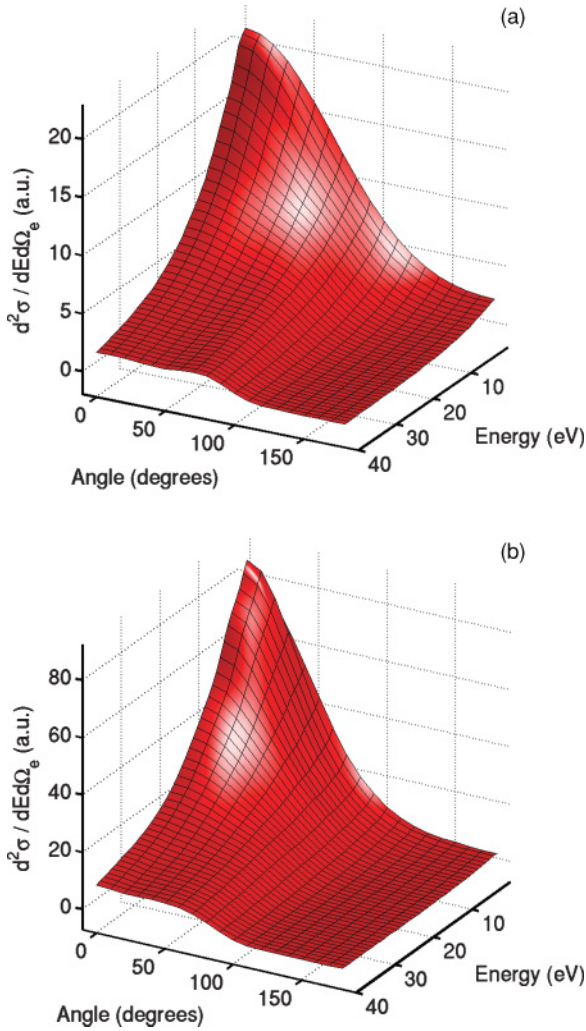


FIG. 14. (Color online) $d^2\sigma/dE d\Omega_e$ for impact of (a) Au^{24+} and (b) Au^{53+} , on He at 3.6 MeV/amu, as calculated in the 165 state CP approximation.

Born IPMB1 approximation continues to show a peak near 80° , this now being the average of the first Born binary peak over all scattered projectile angles and all ejected electron energies. Unlike Fig. 13, which is for specific (low) ejected energies to which the pseudostates have been adapted, see Sec. III, we now see, in the region of the peak, a greater sensitivity to the pseudostate set. This is perhaps not surprising since the need to integrate over all ejected energies requires that the pseudostate set be able to give a good representation of the ejected electron over a wide range of energies. The higher the ejected energy the more partial waves are needed to adequately describe the ejection. In a pseudostate representation these partial waves correspond to the angular momenta of the states included. In the 75 state set only angular momenta from $l = 0$ to $l = 5$ are represented, while in the 165 state set angular momenta from $l = 0$ to $l = 9$ are present. Furthermore, the shape of a cross section as a function of the ejection angle is sensitive to the angular momenta included. Where the ejection angle has been integrated out, as for $d\sigma/dq$ and $d\sigma/dE$ shown in Figs. 16 and 17, this sensitivity is washed out. Obviously, the 165 state results are to be preferred and, although the

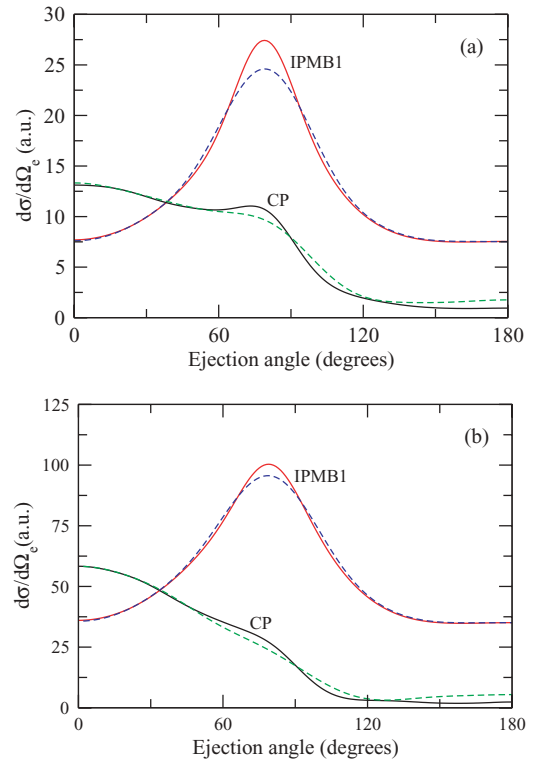


FIG. 15. (Color online) $d\sigma/d\Omega_e$ for (a) Au^{24+} and (b) Au^{53+} , single ionization of He at 3.6 MeV/amu: solid curves (CP and IPMB1), 165 state approximation; dashed curves (CP and IPMB1), 75 state approximation.

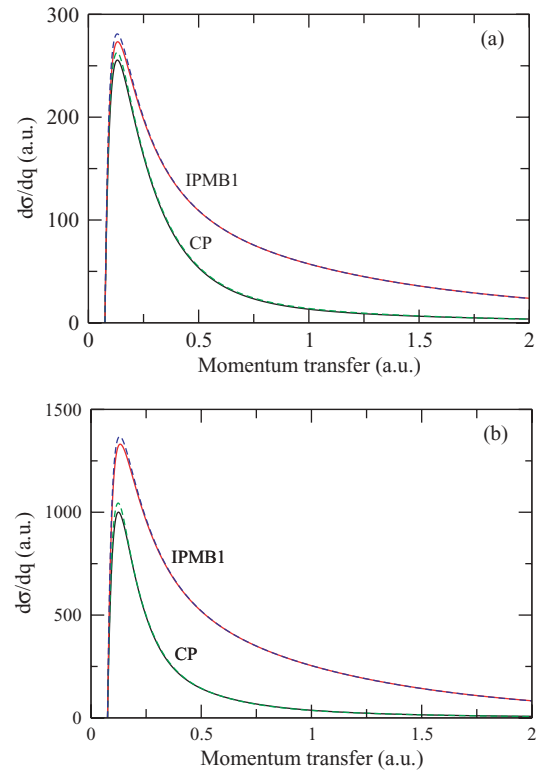


FIG. 16. (Color online) $d\sigma/dq$ for (a) Au^{24+} and (b) Au^{53+} , single ionization of He at 3.6 MeV/amu: solid curves (CP and IPMB1), 165 state approximation; dashed curves (CP and IPMB1), 75 state approximation.

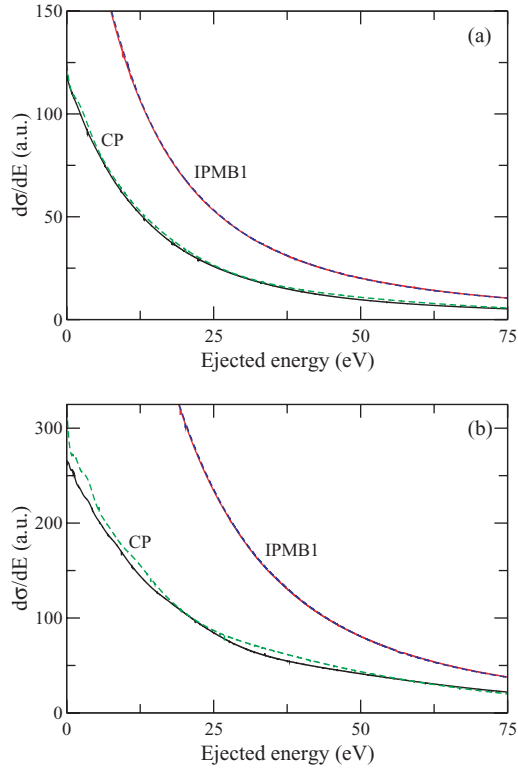


FIG. 17. (Color online) $d\sigma/dE$ for (a) Au^{24+} and (b) Au^{53+} , single ionization of He at 3.6 MeV/amu: solid curves (CP and IPMB1), 165 state approximation; dashed curves (CP and IPMB1), 75 state approximation.

differences between the 75 state and 165 state IPMB1 cross sections are larger than in previous cases, they are not so great as to invalidate confidence in the 165 state calculations.

The differences in the 75 and 165 state CP calculations largely reflect those in the IPMB1 approximation. Like Fig. 13 the CP cross section rises substantially from the backward direction to the forward direction. In the case of Au^{24+} , Fig. 15(a), this rise in the 165 state cross section is interrupted by a small peak near 75° . This peak corresponds to the binary peak in the first Born curve and survives because the postcollisional interaction, which is responsible for the strong rise in the cross section to the forward direction, just fails to suppress it. For the case of Au^{53+} , Fig. 15(b), where the postcollisional interaction is much stronger, the peak is suppressed, but a vestige still remains in the form of a shoulder just above 60° . In Sec. VB2 we commented upon the very small change in curvature of the 10 eV ejection CP cross section for Au^{24+} , Fig. 13(a), which has the same origin (i.e., the competition between the binary peak and the postcollision effect).

2. $d\sigma/dq$ and $d\sigma/dE$

Figure 16 shows $d\sigma/dq$ for Au^{24+} and Au^{53+} . Here we see a small difference in the cross-section peak height between the 75 and 165 state IPMB1 calculations. This difference is reflected in the CP cross sections. Overall, however, the agreement between the 75 and 165 state results is very good. Figure 17 shows $d\sigma/dE$. For Au^{24+} there is good agreement

TABLE I. Total single-ionization cross section (in a.u.).

| | CP(165) | CP(75) | IPMB1(165) | IPMB1(75) |
|-------------------|---------|--------|------------|-----------|
| Au^{24+} | 86 | 86 | 191 | 187 |
| Au^{53+} | 262 | 261 | 787 | 778 |

between the 75 and 165 state calculations. For Au^{53+} there is a noticeable, but not large, difference. The first Born IPMB1 cross section is much larger than CP in the energy range shown.

D. Total single-ionization cross section

In Table I we show the integrated single-ionization cross section in the CP approximation for 165 and 75 states. There is excellent agreement between the two calculations. Also shown are the corresponding first Born IPMB1 results. For bare ions these should scale as $(53/24)^2$ on going from Au^{24+} to Au^{53+} . They do not. This is a result, and a measure, of the screening effect of the projectile electrons.

VI. CONCLUSION

For ionization of He by C^{6+} we have shown, we believe convincingly, that the discrepancy between theory and experiment at 100 MeV/amu in the Y - Z plane geometry of Fig. 1(b) cannot be explained by the projectile-nucleus interaction as was claimed in [34,42]. The theoretical models used in these articles are not well founded. At 2 MeV/amu we get acceptable, but not perfect, agreement with the experiment. From the comparison between the 75 state and 165 state CP calculations it is clear that convergence has been achieved in the CP approximation. Also, the close agreement between the CP numbers and the 3DW-EIS calculations of Foster *et al.* [27] is convincing, especially since the 3DW-EIS approximation is completely different in form from the CP theory.

For ionization by Au^{24+} there is substantial disagreement with the experimental data of [39] but a large degree of consensus between the 75 state CP, 165 state CP, and 3DW-EIS approximations. We believe that in this case theory is reliable.

For Au^{53+} the situation is much more serious. The significant differences between the 75 state and 165 state CP results for the TDCS at $q = 0.65$ and 1.0 a.u. imply lack of convergence at least in the 75 state calculations. Here, there is also disagreement with the 3DW-EIS approximation whose cross section is a factor of 2 smaller in magnitude than the CP predictions. While our confidence in the theoretical position is weak, it is still significantly strong to suggest that an overall factor of 10 difference in normalization between theory and experiment seems unreasonable and that the normalization of the experiment for Au^{53+} needs to be checked.

However, all is not lost. The convergence of the CP calculations is a more subtle matter. We showed in Fig. 9, and again in Fig. 12, that, as the momentum transfer is reduced, the convergence of the CP approximation improves markedly. This is because small momentum transfer collisions are dominated by long-range interactions while large momentum transfer collisions require close encounters. As a consequence,

the average strength of the interaction between the projectile and target reduces with decreasing momentum transfer and so the strain upon the theoretical approximation is relaxed. For positively charged projectiles, as here, part of that “strain” must involve the possibility of charge exchange, which is not *explicitly* incorporated in the approximation used here. It is also clear from Figs. 7, 8, 9, and 12 that the measurements of [39] have been made at momentum transfers where the TDCS is, relatively speaking, small, thus probably also putting pressure upon the experimental technique.

Although convergence of the TDCS may not be so good, it does not follow that convergence of lower-order cross sections, particularly where integrated over q , is as bad. Figures 13, 15, 16, and 17 suggest that the 165 state results for the lower-order cross sections should be quite well converged, while Table I shows that, by the time we get to the total single-ionization cross section, convergence is no longer a problem.

While experimental measurements of the TDCS remain the priority, experimental investigation of some of the lower-order cross sections will be valuable, if only to check the experiment against more robust theoretical predictions. Of particular interest will be measurements of $d^2\sigma/dEd\Omega_e$ (Fig. 13) and $d\sigma/d\Omega_e$ (Fig. 15), which show the strong PCI effect. Of these, the cross section $d\sigma/d\Omega_e$ for Au²⁴⁺, Fig. 15(a), will be especially interesting as it shows, in the form of a bump near 75°, a clear competition between the binary peak dynamics and the post collisional interaction.

ACKNOWLEDGMENTS

MMcG acknowledges support from the European Social Fund and Queen’s University Belfast. DA and JRM acknowledge financial support from the Brazilian agencies CNPq, Capes, and Fapemig.

-
- [1] P. D. Fainstein, V. H. Ponce, and R. D. Rivarola, *J. Phys. B* **21**, 287 (1988).
- [2] P. D. Fainstein, V. H. Ponce, and R. D. Rivarola, *J. Phys. B* **24**, 3091 (1991).
- [3] J. O. P. Pedersen, P. Hvelplund, A. G. Petersen, and P. D. Fainstein, *J. Phys. B* **23**, L597 (1990).
- [4] J. O. P. Pedersen, P. Hvelplund, A. G. Petersen, and P. D. Fainstein, *J. Phys. B* **24**, 4001 (1991).
- [5] N. Stolterfoht, H. Platten, G. Schiwietz, D. Schneider, L. Gulyás, P. D. Fainstein, and A. Salin, *Phys. Rev. A* **52**, 3796 (1995).
- [6] Y. D. Wang, V. D. Rodríguez, C. D. Lin, C. L. Cocke, S. Kravis, M. Abdallah, and R. Dörner, *Phys. Rev. A* **53**, 3278 (1996).
- [7] S. D. Kravis, M. Abdallah, C. L. Cocke, C. D. Lin, M. Stöckli, B. Walch, Y. D. Wang, R. E. Olson, V. D. Rodríguez, W. Wu, M. Pieksma, and N. Watanabe, *Phys. Rev. A* **54**, 1394 (1996).
- [8] M. Abdallah, S. Kravis, C. L. Cocke, Y. Wang, V. D. Rodríguez, and M. Stöckli, *Phys. Rev. A* **56**, 2000 (1997).
- [9] L. C. Tribedi, P. Richard, Y. D. Wang, C. D. Lin, L. Gulyás, and M. E. Rudd, *Phys. Rev. A* **58**, 3619 (1998).
- [10] L. C. Tribedi, P. Richard, Y. D. Wang, C. D. Lin, R. E. Olson, and L. Gulyás, *Phys. Rev. A* **58**, 3626 (1998).
- [11] L. C. Tribedi, P. Richard, L. Gulyás, and M. E. Rudd, *Phys. Rev. A* **63**, 062724 (2001).
- [12] C. J. Wood, C. R. Feeler, and R. E. Olson, *Phys. Rev. A* **56**, 3701 (1997).
- [13] R. E. Olson, C. J. Wood, H. Schmidt-Böcking, R. Moshhammer, and J. Ullrich, *Phys. Rev. A* **58**, 270 (1998).
- [14] R. E. Olson and J. Fiol, *J. Phys. B* **34**, L625 (2001).
- [15] R. E. Olson and J. Fiol, *J. Phys. B* **36**, L365 (2003).
- [16] S. Otranto, R. E. Olson, and J. Fiol, *J. Phys. B* **39**, L175 (2006).
- [17] J. Fiol, S. Otranto, and R. E. Olson, *J. Phys. B* **39**, L285 (2006).
- [18] R. Moshhammer, A. Perumal, M. Schulz, V. D. Rodríguez, H. Kollmus, R. Mann, S. Hagmann, and J. Ullrich, *Phys. Rev. Lett.* **87**, 223201 (2001).
- [19] M. Schulz, R. Moshhammer, D. H. Madison, R. E. Olson, P. Marchalant, C. T. Whelan, H. R. J. Walters, S. Jones, M. Foster, H. Kollmus, A. Cassimi, and J. Ullrich, *J. Phys. B* **34**, L305 (2001).
- [20] M. Schulz, R. Moshhammer, A. N. Perumal, and J. Ullrich, *J. Phys. B* **35**, L161 (2002).
- [21] D. Madison, M. Schulz, S. Jones, M. Foster, R. Moshhammer, and J. Ullrich, *J. Phys. B* **35**, 3297 (2002).
- [22] M. Schulz, R. Moshhammer, D. Fisher, H. Kollmus, D. H. Madison, S. Jones, and J. Ullrich, *Nature (London)* **422**, 48 (2003).
- [23] D. Fischer, R. Moshhammer, M. Schulz, A. Voitkiv, and J. Ullrich, *J. Phys. B* **36**, 3555 (2003).
- [24] M. Schulz, R. Moshhammer, D. Fischer, and J. Ullrich, *J. Phys. B* **36**, L311 (2003).
- [25] D. Fischer, A. B. Voitkiv, R. Moshhammer, and J. Ullrich, *Phys. Rev. A* **68**, 032709 (2003).
- [26] D. H. Madison, D. Fischer, M. Foster, M. Schulz, R. Moshhammer, S. Jones, and J. Ullrich, *Phys. Rev. Lett.* **91**, 253201 (2003).
- [27] M. Foster, D. H. Madison, J. L. Peacher, M. Schulz, S. Jones, D. Fischer, R. Moshhammer, and J. Ullrich, *J. Phys. B* **37**, 1565 (2004).
- [28] M. Schulz, R. Moshhammer, D. Fischer, and J. Ullrich, *J. Phys. B* **37**, 4055 (2004).
- [29] M. Dürr, B. Najjari, M. Schulz, A. Dorn, R. Moshhammer, A. B. Voitkiv, and J. Ullrich, *Phys. Rev. A* **75**, 062708 (2007).
- [30] M. F. Ciappina, W. R. Cravero, and C. R. Garibotti, *J. Phys. B* **36**, 3775 (2003).
- [31] M. F. Ciappina and W. R. Cravero, *J. Phys. B* **39**, 1091 (2006).
- [32] M. F. Ciappina and W. R. Cravero, *J. Phys. B* **39**, 2183 (2006).
- [33] V. D. Rodríguez, *Nucl. Instrum. Methods B* **205**, 498 (2003).
- [34] F. Járαι-Szabó and L. Nagy, *J. Phys. B* **40**, 4259 (2007).
- [35] W. Schmitt, R. Moshhammer, F. S. C. O’Rourke, H. Kollmus, L. Sarkadi, R. Mann, S. Hagmann, R. E. Olson, and J. Ullrich, *Phys. Rev. Lett.* **81**, 4337 (1998).
- [36] J. Fiol and R. E. Olson, *Nucl. Instrum. Methods B* **205**, 474 (2003).

- [37] J. Fiol and R. E. Olson, *J. Phys. B* **37**, 3947 (2004).
- [38] R. E. Olson and J. Fiol, *Phys. Rev. Lett.* **95**, 263203 (2005).
- [39] M. Foster, D. H. Madison, J. L. Peacher, and J. Ullrich, *J. Phys. B* **37**, 3797 (2004).
- [40] P. D. Fainstein and L. Gulyás, *J. Phys. B* **38**, 317 (2005).
- [41] R. T. Pedlow, S. F. C. O'Rourke, and D. S. F. Crothers, *Phys. Rev. A* **72**, 062719 (2005).
- [42] M. Schulz, M. Dürr, B. Najjari, R. Moshhammer, and J. Ullrich, *Phys. Rev. A* **76**, 032712 (2007).
- [43] M. McGovern, D. Assafrão, J. R. Mohallem, Colm T. Whelan, and H. R. J. Walters, *Phys. Rev. A* **79**, 042707 (2009).
- [44] M. McGovern, D. Assafrão, J. R. Mohallem, C. T. Whelan, and H. R. J. Walters, *Phys. Rev. A* **81**, 032708 (2010).
- [45] M. McGovern, Ph.D. thesis, Queen's University, Belfast, 2009.
- [46] A. Igarashi, L. Gulyás, and P. D. Feinstein, *Eur. Phys. J. D* **42**, 73 (2007).
- [47] In this approximation one electron is frozen into the $1s$ orbital of He^+ but the other electron can be excited to any state. This state and the overall state of the He atom can then be labeled by the hydrogenic quantum numbers nlm .
- [48] M. E. Rose, *Elementary Theory of Angular Momentum* (Wiley, New York, 1957).
- [49] The dependence of $a_{nlm}(t, \mathbf{b})$ on the direction of \mathbf{b} may be factored out as $a_{nlm}(t, \mathbf{b}) = e^{-im\phi_b} \bar{a}_{nlm}(t, b)$ where ϕ_b is the azimuthal angle of \mathbf{b} about \mathbf{v}_0 , see [43].
- [50] By adjusting the exponential parameter λ_l in (16). The values of λ_l are tabulated in [45].
- [51] A. D. McLean and R. S. McLean, *At. Data Nucl. Data Tables* **26**, 197 (1981).